CONF-950686--1

SAND94-2298C

DYNAMIC BRITTLE MATERIAL RESPONSE BASED ON A CONTINUUM DAMAGE MODEL

E. P. Chen
Material and Structural Mechanics Department
Sandia National Laboratories
Albuquerque, New Mexico

ABSTRACT

The response of brittle materials to dynamic loads was studied in this investigation based on a continuum damage model. The damage mechanism in this model has been selected to be the interaction and growth of subscale cracks. Briefly, the cracks are activated by bulk tension and the density of activated cracks are described by a Weibull statistical distribution. The moduli of a cracked solid derived by Budiansky and O'Connell are then used to represent the global material degradation due to subscale cracking. This continuum damage model was originally developed to study rock fragmentation and was modified in the present study to improve on the post-limit structural response. The model was implemented into a transient dynamic explicit finite element code PRONTO 2D and then used for a numerical study involving the sudden stretching of a plate with a centrally located hole. Numerical results characterizing the dynamic responses of the material were presented. The effect of damage on dynamic material behavior was discussed.

INTRODUCTION

An important aspect of many applications employing brittle materials involves the understanding of the dynamic behavior of these materials under rapidly applied loads. Typically, many brittle materials have a pre-existing flaw structure. Accurate predictions of the dynamic responses of these materials require an understanding of their dynamic fracture behavior. Many observed phenomena in these materials, such as strain-rate effects, crack-tip damage, tension softening, etc., cannot be explained by classical elastodynamic fracture mechanics. An approach based on continuum damage mechanics (Taylor, Chen and Kuszmaul, 1986; Chen, 1986; and Chen and Taylor, 1986) has been employed by the author and his coworkers to treat dynamic brittle fracture problems. In this model, the material is approximated as a continuum with a random distribution of sub-scale cracks. The moduli of the material follows those of a cracked solid given by the equations of Budiansky and O'Connell (1976). The activation of these cracks by the applied tensile load produces progressive damage to the material. In the continuum scale, accumulation of damage is reflected by the softening of the material moduli. Under compressive loads, the material is assumed to behave as an elastic/perfectly plastic solid. The tensile strain-rate effect has been

DISCLAIMER

Portions of this document may be illegible in electronic image products. Images are produced from the best available original document.

explicitly included in the model. The model has been applied to explosive rock fragmentation and dynamic concrete fracturing, and reasonable correlations between calculated and measured data were obtained (Taylor, Chen and Kuszmaul, 1986; Chen, 1986; Chen and Taylor, 1986; and Thorne, 1990 & 1991).

Applications of the damage model to field problems have identified three areas of improvements. The first is concerned with the inadequacy of elastic/perfectly plastic representation in compression because many brittle materials exhibit pressure-dependent inelastic behavior. Another area concerns with the dilute crack concentration formulation in Budiansky and O'Connell's model (1976) which limits the crack density in a representative volume element. Lastly, the tension damage and compression inelasticity formulation are uncoupled and independent of each other. In this investigation, the damage model was modified to reflect improvements in the above areas. A linear pressure-dependent Drucker-Prager model (1952) has been implemented to replace the elastic/perfectly plastic representation. To extend the range of crack densities, an expression based on percolation theory (Englman and Jaeger, 1987) has been used to approximate the crack density definition in the Budiansky and O'Connell model. Coupling of the tension damage and compression inelasticity is accomplished by the introduction of a unloading/reloading parameter. Details of these improvements are described in the paper. The improved continuum damage model has been implemented into the transient dynamic finite element code PRONTO 2D (Taylor and Flanagan, 1987) to facilitate numerical computations.

To demonstrate the utility of the improved damage model, an example involving a plate with a centrally located hole which is suddenly being stretched along its edges is considered. Because of complex wave interactions, the maximum damage and strains occur at a different location along the hole boundary from the corresponding quasi-static case. Comparisons between the results from the damage model and its corresponding elastic case are made to show the effect of damage accumulation. Strain and damage contour plots are presented to show localization. Strain softening is observed from bulk strain versus pressure plots around the hole boundary. Discussions of the implications of these results are presented.

CONTINUUM DAMAGE MODEL DESCRIPTION

The basic assumption of the damage model is that the material is permeated by an array of randomly distributed cracks which grow and interact with one another under tensile loading. The model does not attempt to treat each individual crack, but rather treats the growth and interaction of cracks as internal state variables which represent damage accumulation in the material. The damage is reflected in the degradation of the material stiffness following the equations derived by Budiansky and O'Connell (1976) for a random array of penny-shaped cracks in an isotropic elastic medium

$$\frac{\overline{K}}{K} = 1 - \frac{16}{9}\left(\frac{1-\nu^2}{1-2\nu}\right)C_d \tag{1}$$

$$\frac{\overline{G}}{G} = 1 - \frac{32}{45}\frac{(1-\nu)(5-\nu)}{(2-\nu)}C_d \tag{2}$$

$$\frac{\overline{E}}{E} = 1 - \frac{16}{45}\frac{\left(1-\nu^2\right)(10-3\nu)}{(2-\nu)}C_d \tag{3}$$

where K, G, E and ν are material bulk modulus, shear modulus, Young modulus and Poisson's ratio, respectively. Barred quantities such as $\overline{K}$ represent degraded properties and C_d is the crack density parameter. Additionally, the crack density parameter is related to the virgin and damaged Poisson's ratio through:

$$C_d = \frac{45}{16}\frac{(\nu-\nabla)\,(2-\nabla)}{\left(1-\nabla^2\right)[10\nu-\nabla\,(1+3\nu)]} \tag{4}$$

The damage variable is defined as

$$D = \frac{16}{9}\left(\frac{1-\nabla^2}{1-2\nabla}\right)C_d \tag{5}$$

such that $\overline{K} = K\,(1 - D)$. The crack density parameter is assumed to be proportional to the product of N, the number of cracks per unit volume, and a^3, the cube of the average crack dimension in a representative volume. Following Grady and Kipp (1980), N is expressed as a Weibull statistical distribution function activated by the bulk strain measure $\varepsilon_v = (\varepsilon_x + \varepsilon_y + \varepsilon_z)/3$, according to

$$N = k\left(\varepsilon_v\right)^m \tag{6}$$

in which k and m are material constants to be determined from strain rate dependent tensile fracture stress data. The average crack dimension a, is estimated from the nominal fragment diameter for dynamic fragmentation in a brittle material (Grady, 1980) as

$$2a = \left(\frac{\sqrt{20}K_{IC}}{\rho C\dot{\varepsilon}_{vmax}}\right)^{\frac{2}{3}} \tag{7}$$

where ρ is the mass density, C is the uniaxial wave speed $(E/\rho)^{1/2}$, and K_{IC} is the fracture toughness of the material. Also, $\dot{\varepsilon}_{vmax}$ is the maximum volumetric strain rate experienced by the representative volume element. Equations (1) through (5) can also be cast into rate form to relate stress and strain rates. When bulk tension occurs in the material, it is possible to calculate, at each time step, the crack density parameter C_d by making use of Equations (6) and (7) and then damage parameter D through Equation (5). The material stiffness is then degraded according to Equations (1) through (5). In compression, the material behaves as an elastic/perfectly plastic solid. Details of the model development are given in Taylor, Chen and Kuszmaul (1986) and will not be repeated here.

Modifications have been made to the above model to render it a more versatile tool. Because the equations derived by Budiansky and O'Connell (1976) are limited to dilute crack concentrations, the crack density parameter has a limiting value of 9/16. To extend the range of crack densities, an expression based on percolation theory (Englman and Jaeger, 1987)

$$\nabla = \nu\exp\left(-\frac{16}{9}\beta C_d\right) \quad , \qquad 0 \le \beta \le 1 \tag{8}$$

was used to approximate Equation (4). The value of β controls the unloading and reloading behavior and relaxes the restriction of elastic unloading in the original model.

For many brittle solids, pressure-dependent inelastic response under compressive loads is observed. An improvement is made by extending the elastic/perfectly plastic compressive response to one that employs a Drucker-Prager yield surface (1952):

$$F = \bar{\sigma}^2 - \left(c_1 + c_2 P\right)^2 = 0 \tag{9}$$

with $\bar{\sigma}$ the effective stress, P the mean stress and c_1 and c_2 material constants determined from experimental data. To avoid too much dilation, a von Mises flow rule of the type

$$\dot{\varepsilon}_{ij}^{p} = \dot{\lambda}\frac{s_{ij}}{\sqrt{s_{ij}s_{ij}}} \tag{10}$$

is adopted. In Equation (10), $\dot{\varepsilon}_{ij}^{p}$ is the plastic strain rate tensor, $\dot{\lambda}$ is the plastic loading rate parameter, and s_{ij} is the deviatoric stress tensor.

Without going into more details, this modified damage model have been vectorized and implemented into the explicit finite element code PRONTO 2D (Taylor and Flanagan, 1987) for efficient computations.

CHARACTERISTICS OF THE DAMAGE MODEL

Characteristics of the continuum damage model described are examined here for concrete. The concrete properties used are those for the high strength (140.0 MPa unconfined compressive strength) concrete slab tested in Hanchak et al. (1992). Nominal material properties such as the mass density, the Young's modulus, the Poisson's ratio and the fracture toughness are taken to be 2520 kg/m^3, 20.68 GPa, 0.18 and 2.747 MPa-m$^{1/2}$, respectively. Shear strength was measured by Hanchak et al. (1992) and an linear relationship of τ = 220.8 + 0. 313 p (MPa) was fit to the data, Fig. 1. The fitted curve is used in the

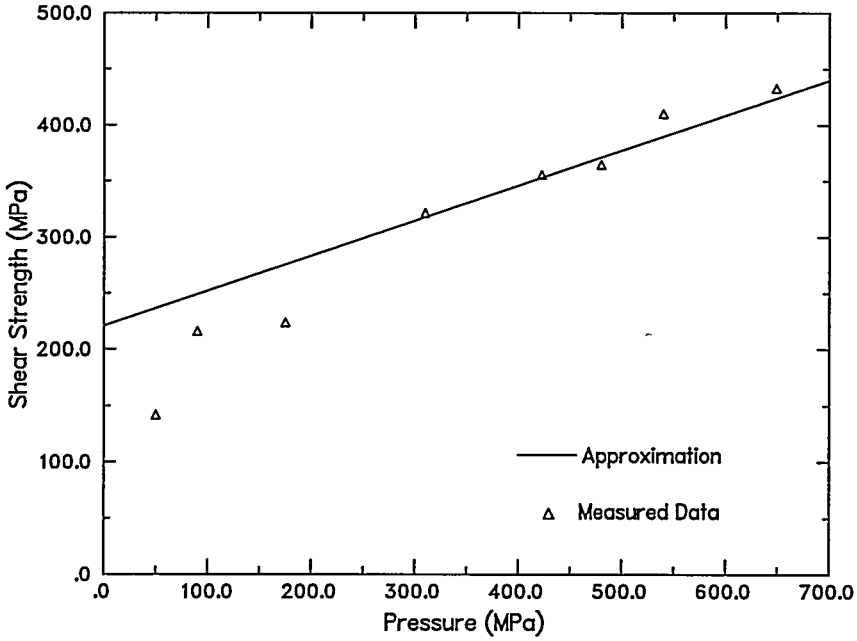

Figure 1. Concrete shear strength versus pressure data.

numerical analysis. Strain-rate dependent tensile fracture stress data are required to determine the constants k and m in Equation (6). In lieu of measured data, it is possible to estimate this data using an expression derived in Kipp, Grady and Chen (1980) for the tensile fracture stress σ_c:

$$\sigma_c = \left(\frac{9\pi E K_{IC}^2}{16 N_s^2 C_s} \right)^{\frac{1}{3}} \dot{\varepsilon}^{\frac{1}{3}} \tag{11}$$

where N_s is a shape factor (1.12 for penny-shaped cracks) and C_s is the shear wave velocity of the material. Based on this equation and the material properties given above, m and k are determined to be 6.0 and 5.753 $10^{21}/m^3$, respectively.

Using these material properties and 0.5 for β, the response of the concrete under bulk tension can now be examined. Fig. 2 shows the pressure-volumetric strain relationship under uniaxial homogeneous straining

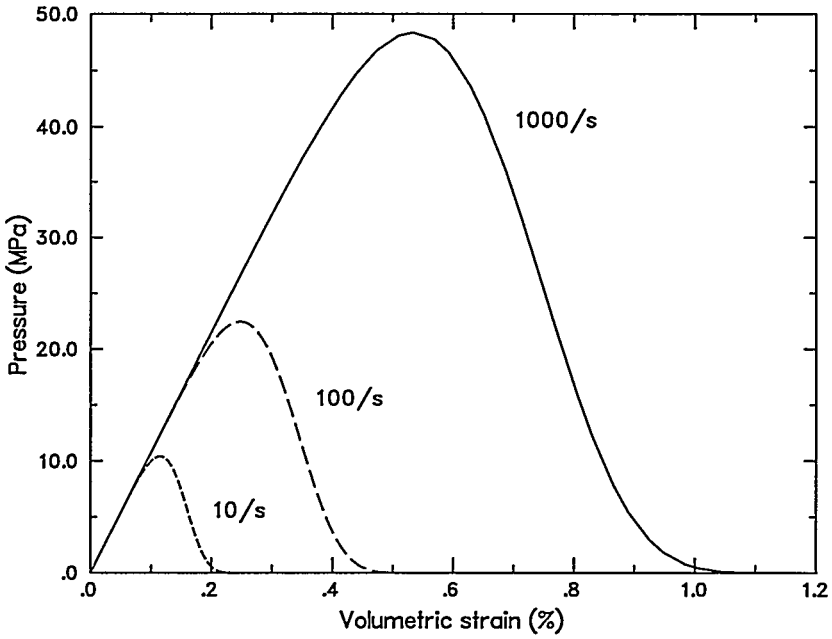

Figure 2. Concrete bulk response under tension.

for three strain rates. In this figure, positive pressure denotes bulk tension. Strain-softening is observed as a consequence of the micro-cracking damage accumulation. The material's capability to carry bulk tension increases with the strain rate. Damage accumulation as a function of volumetric strain is shown in Fig. 3. The loading/unloading/reloading behavior for 1000/s strain rate is exhibited in Fig. 4 and 5 in terms of pressure- and damage-volumetric strain plot, respectively. It is seen that the damage evolution is an irreversible process. During reloading, no more damage accumulation will take place until the strain level have exceeded the previous maximum. The value for β controls the unloading response. For β=0, elastic unloading along the damaged bulk modulus will result. For β=1, unloading is along the original bulk modulus similar to elastic/plastic behavior. For β between 0 and 1, a combined damage/plastic unloading

response results. The effect of β is illustrated in Fig. 6.

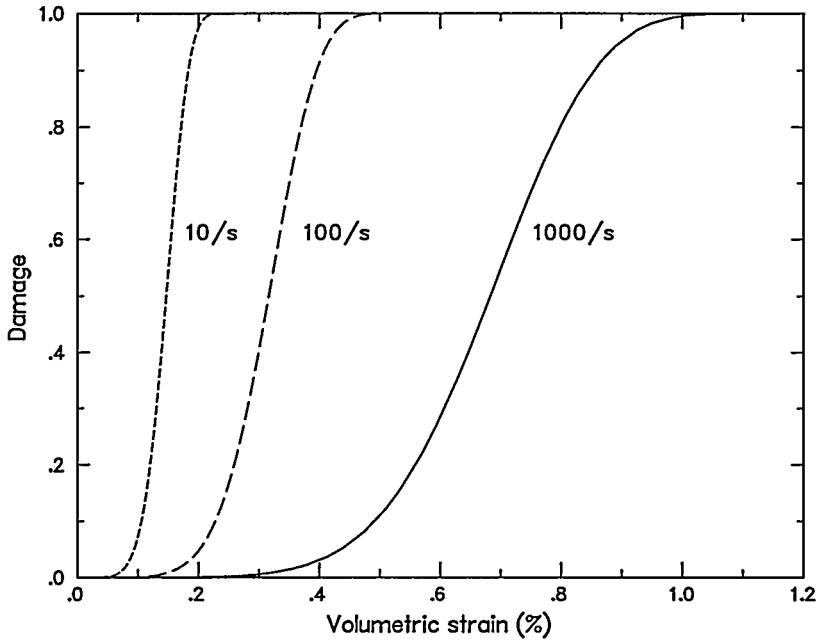

Figure 3. Damage versus volumetric strain plot.

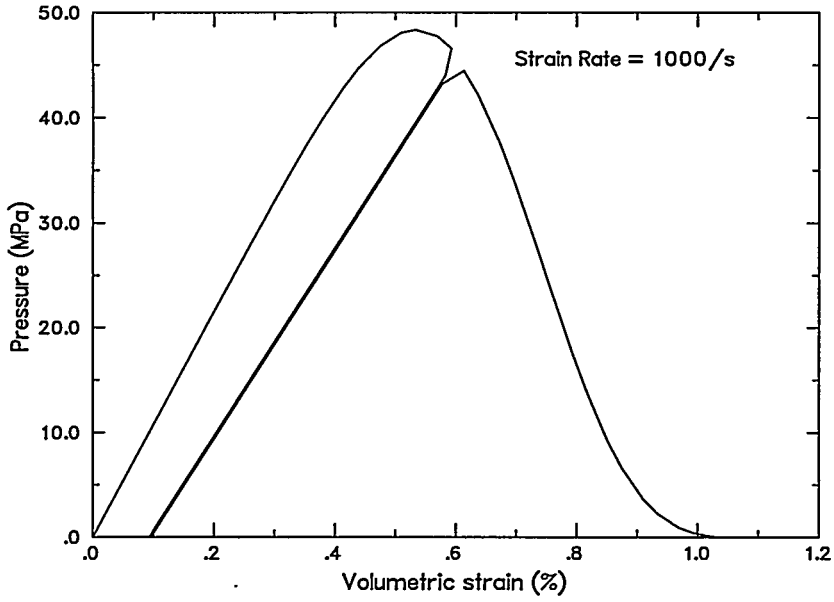

Figure 4. Cyclic bulk tension response of concrete.

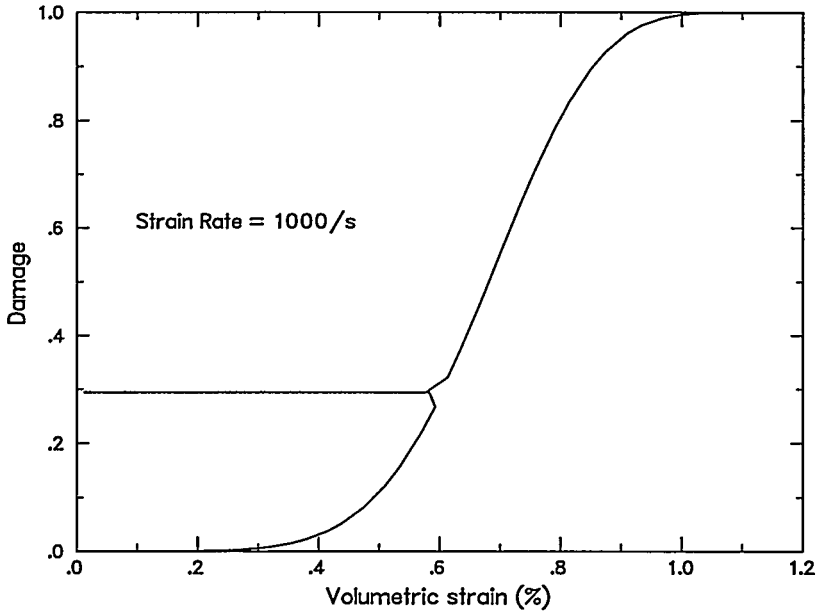

Figure 5. Cyclic damage behavior.

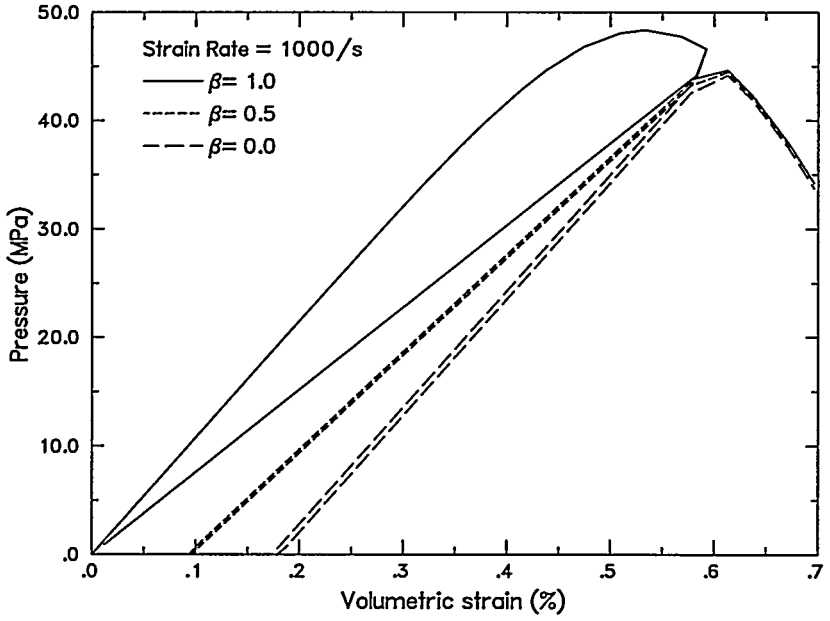

Figure 6. Effect of β on unloading.

EXAMPLE PROBLEM CALCULATION

To demonstrate the dynamic behavior defined by the modified damage model, an example problem involving the sudden stretching of a plate with a centrally located hole is selected. Consider the 0.2 m by 0.4 m rectangular plate with a 0.1 m diameter hole in the center in Fig. 7. A step tensile pulse is applied

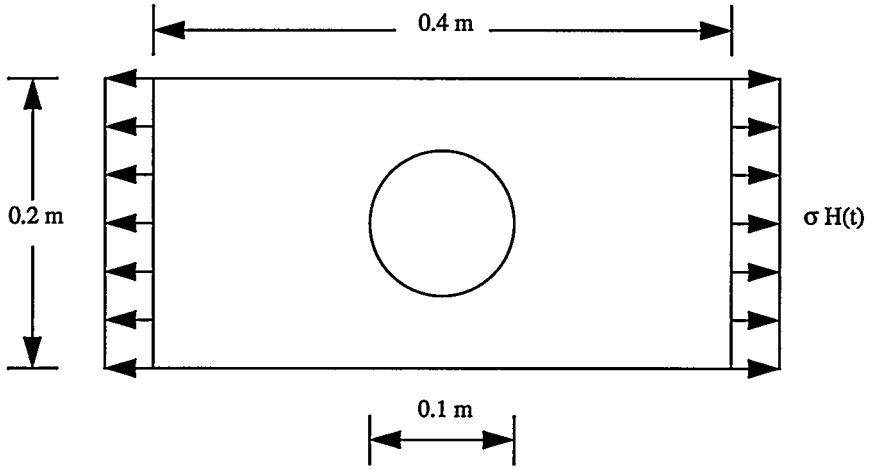

Figure 7. Schematic drawing of the example problem.

symmetrically to the left and right edge of the plate. The plate consists of the same concrete material as the one given in the last section. For numerical calculations, the pulse is given a strength of 10.0 MPa. The modified damage model as implemented in the finite element code PRONTO 2D is used to obtain the dynamic response of the plate. The plane strain condition is assumed to prevail. Because of symmetry, only one quarter of the geometry in Fig. 7 needs to be included in the finite element mesh. This is shown in Fig. 8 where a 90-degree rotation has been made. The mesh includes 2,800 quadrilateral elements and 2,921 nodes. Based on quasi-static results, high level of tensile stress is expected to occur along the hole boundary at point A, Fig. 8. Therefore, fine meshing is placed around the hole from point A to B in order to capture the sharp stress gradient. There are 40 elements in the first ring along the boundary of the hole from point A to B and these elements have numbers from 1 to 1561 with an increment of 40.

Before the damage model is applied, the elastodynamic case is considered first to establish a reference solution. Fig. 9 shows the pressure history plots at five element locations along the boundary of the hole between point A and B which are defined in Fig. 8. Element 1 is at point A and element 1561 is at point B, while the other element numbers 401, 801, and 1201 are at equal distances between points A and B. Based on the concrete properties in the last section, a longitudinal wave velocity of 2,985 m/s is calculated. Thus, a reflected compressional wave will arrive at the center of the plate at approximately 0.2 ms. Because the main purpose is to examine the tensile damage behavior, the calculation is terminated at 0.2 ms. It is observed that at each one of these locations, the material is at rest prior to the arrival of the wave front. The sustained tensile pulse then stretches the material and the material is being loaded in tension (negative pressure) until the reflected wave arrives from the other end and the material unloads. In between, diffracted and reflected waves from the hole boundary and the side edges of the plate also have an effect on pressure behavior and contributed to the wavy appearance of the curves in Fig. 9. The geometry effect dictates the magnitude of the pressures at these locations.

Similar pressure history curves for the damage model are shown in Fig. 10. Initially, similar behavior as the elastic case is observed. However, because tensile fractures occur during the wave loading process,

which in term redistribute pressures in the material, the tensions in the material can not attain the levels

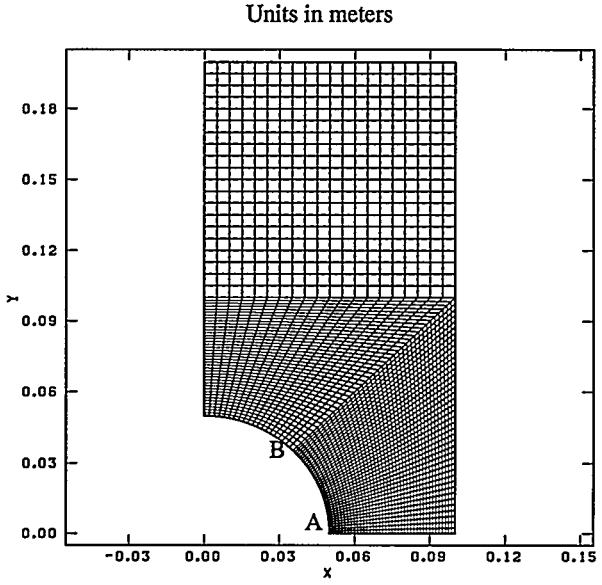

Figure 8. Finite element mesh of the example problem.

reached by its elastic counterpart. Tensile fractures cause premature unloading of the material and this is shown in Fig. 10.

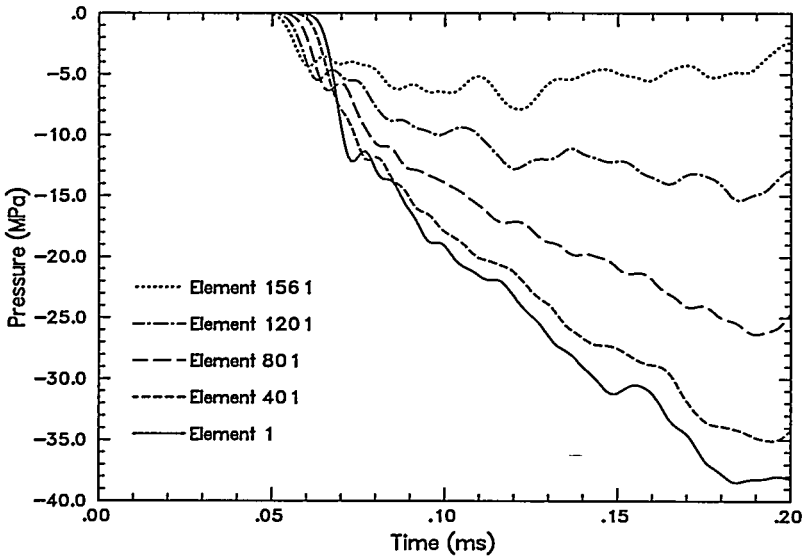

Figure 9. Pressure history at various locations - elastic case.

The evolution of damage D is depicted in the shaded contour plots in Fig. 11. Note that (1-D) represents

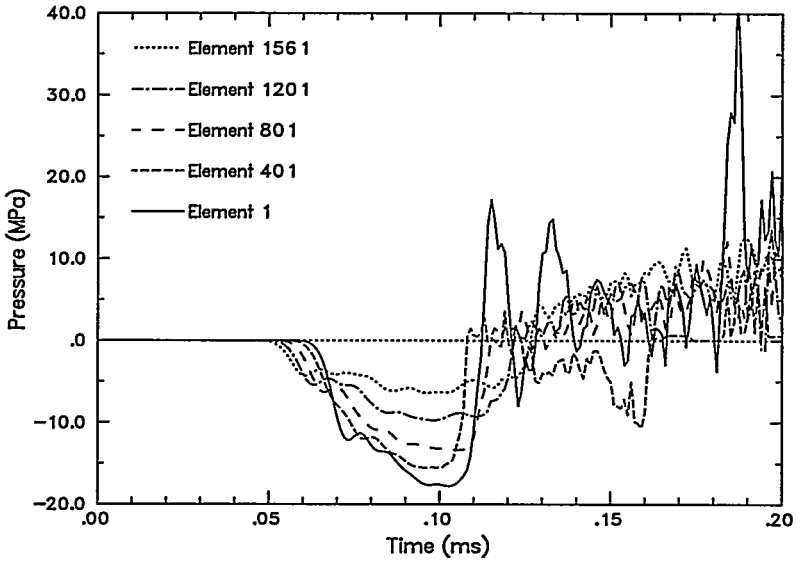

Figure 10. Pressure history at various locations - damage model.

the factor of the degraded bulk modulus divided by the original one. Four snapshots of the plate,

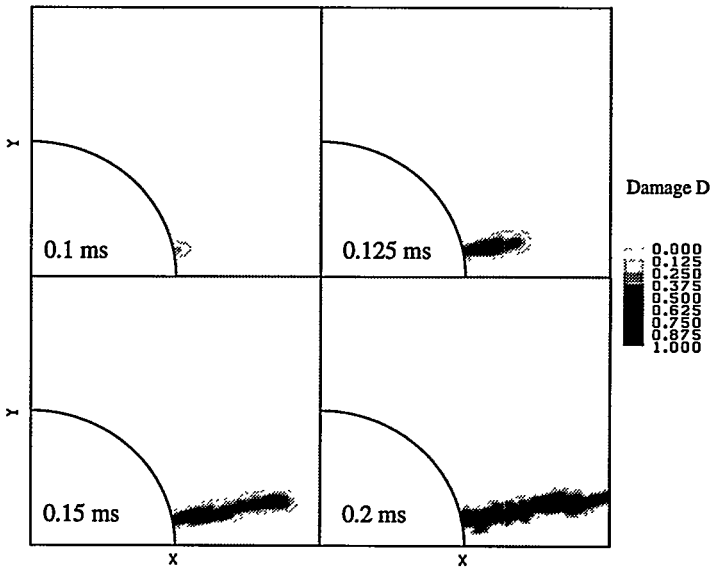

Figure 11. Damage evolution in the plate.

corresponding to times 0.1, 0.125, 0.15, and 0.2 ms after the tensile pulse is applied, are shown. Because the damage localizes around the hole, only the lower 0.1 m by 0.1 m square area of the plate (see Fig. 8) is included in Fig. 11. The damage localizes into a band as shown in Fig. 11. The evolution of bulk strain ε_v is shown in Fig. 12. Similar behavior to that in Fig. 11 is observed. It is interesting to note that the

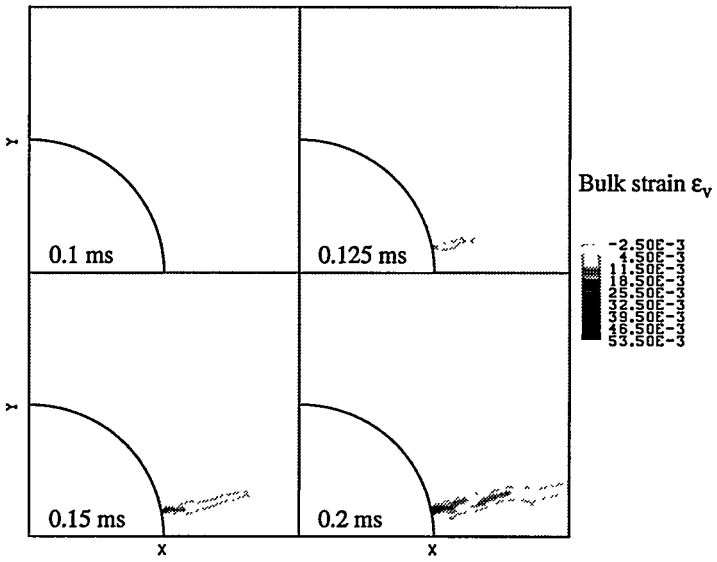

Figure 12. Bulk strain evolution in the plate.

damage does not initiate from point A in Fig. 8, the corresponding maximum tensile stress location under quasi-static loads. This seems to contradict with the pressure history plots in Fig. 10 because the maximum tension occurs at point A (element 1). This apparent contradiction can be explained by the strain-rate dependent characteristic of the damage model. Figure 13 shows the bulk strain-rate history plots at the locations of elements 1, 401, and 801. Elements 1201 and 1561 have been excluded because their behavior is similar to element 801 and the inclusion of these elements will not yield additional information. The curves in Fig. 13 are terminated at 0.11 ms such that the initial differences in strain-rate can clearly be observed. At the time when the tensile stress attains its maximum value, approximately 0.1 ms after the application of the tensile pulse, element 1 has experienced a higher bulk strain-rate (56 /s) than element 401 (33 /s) and element 801 (30 /s). Thus, up to 0.1 ms, element 1 has a higher strength than elements 401 and 801. The dependence of strength on bulk strain-rate is a characteristic of the present damage model and can be observed from the plots in Fig. 2. Hence, although higher tensile stress is attained at element 1, less damage is accumulated at this location than that for element 401. This is evidenced by the damage history plots in Fig. 14. The evolution of damage can be observed from Fig. 14 which also follows the pressure history in Fig. 10. Damage starts to accumulate when the tensile wave front arrives at the element location. Damage is irreversible and can only be accumulated under tension. Therefore, damage remains at a constant value during unloading. The effect of damage can also be observed from the pressure versus bulk strain plots in Figs. 15 for elements, 1, 401, and 801. The curve for element 1 shows that initially, no damage is accumulated and the material behaves elastically. Continued tension produces damage and the curve deviates from linearity. Unloading occurs prior to the attainment of peak load and material unloads along the degraded bulk modulus. Similar behavior but at a lower

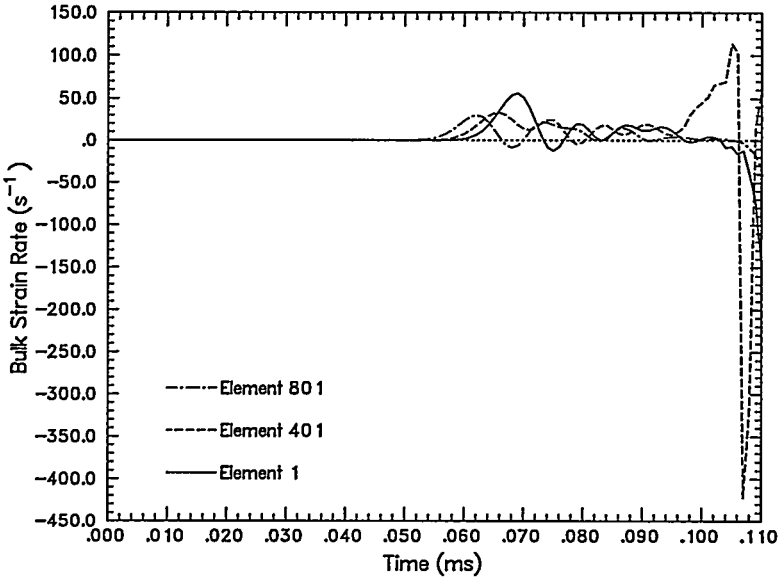

Figure 13. Bulk strain history plots.

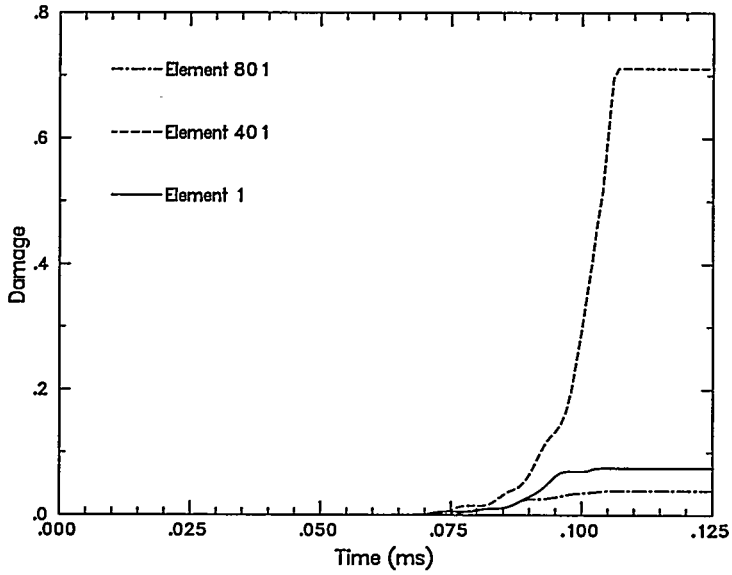

Figure 14. Damage history plots.

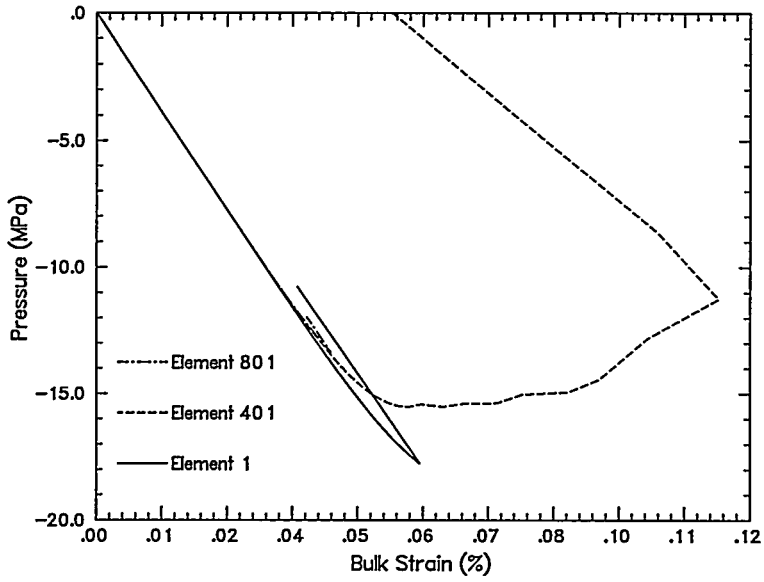

Figure 15. Pressure versus bulk strain plots.

pressure magnitude is observed for element 801. For element 401, unloading occurs after the peak load is attained and tension softening behavior is observed.

SUMMARY

The dynamic response of brittle materials is investigated in this paper based on a continuum damage model. The model assumes pre-existing flaws and the growth and interaction of these flaws under applied tension degrade material stiffness. The degree of degradation is defined as the material damage. The framework of this model was developed previously by the author and his co-workers. However, three major improvements have been added to make the model a more versatile tool. The modified model has been implemented into the transient dynamic finite element PRONTO 2D. Material characteristics of the model was presented for a concrete panel.

An example problem involving a concrete plate with a centrally located hole was considered to demonstrate the dynamic structural response based on the damage model. Damage localization and strain softening were observed. An interesting result was obtained where the location of maximum damage under dynamic loads does not correspond to the one under quasi-static loads. This can be explained by the wave interactions and the strain-rate dependent characteristic of the damage model.

ACKNOWLEGEMENT

This work was funded by the Laboratory Directed Research and Development Program, Sandia National Laboratories, under the auspices of the U. S. Department of Energy under Contract Number DE-AC04-94AL85000.

REFERENCES

Budiansky, B. and O'Connell, R. J., 1976, "Elastic Moduli of a Cracked Solid," International Journal of Solids and Structures, Vol. 12, pp. 81-97.

Chen, E. P., 1986, "Continuum Damage Mechanics Studies on the Dynamic Fracture of Concrete," in *Cement-Based Composites: Strain Rate Effects on Fracture,* S. Mindess and S. P. Shah, Editors, Materials Research Society Symposia Proceedings Volume 64, Materials Research Society, Pittsburgh, Pennsylvania, pp.63-77.

Chen, E. P. and Taylor, L. M., 1986, "Fracture of Brittle Rock Under Dynamic Loading Conditions," in *Fracture Mechanics of Ceramics,* Volume 7, R. C. Bradt, A. G. Evans, D. P. H. Hasselman, and F. F. Lange, Editors, Plenum press, New York, pp.175-186.

Drucker, D. C. and Prager, W., 1952, "Soil Mechanics and Plastic Analysis or Limit Design," Quarterly of Applied Mathematics, Vol. 10, pp. 157-165.

Englman, R. and Jaeger, Z., 1987, "Theoretical Aids for the Improvement of Blasting Efficiencies in Oil Shale and Rocks," AP-TR-12/87, Soreq Nuclear Research Center, Yavne, Israel.

Grady, D. E., 1980, "The Mechanics of Fracture under High-Rate Stress Loading," Preprints of the William Prager Symposium on *Mechanics of Geomaterials: Rocks, Concrete and soils,* Z. P. Bazant, Editor, Northwestern University, Evanston, Illinois, pp. 149-188.

Grady, D. E. and Kipp, M. E., 1980, "Continuum Modeling of Explosive Fracture in Oil Shale," International Journal of Rock Mechanics and Mining Science, Vol. 17, pp. 147-157.

Hanchak, S. J., Forrestal, M. J., Young, E. R., and Ehrgott, J. Q., 1992, "Perforation of Concrete Slabs with 48 MPa and 140 MPa Unconfined Compressive Strengths," International Journal of Impact Engineering, Vol. 12, pp. 1-7.

Kipp, M. E., Grady, D. E. and Chen, E. P., 1980, "Strain-Rate Dependent Fracture Initiation," International Journal of Fracture, Vol. 16, pp. 471-478.

Taylor, L. M., Chen, E. P., and Kuszmaul, J. S., 1986, "Microcrack-Induced Damage Accumulation in Brittle Rock under Dynamic Loading," Journal of Computer Methods in Applied Mechanics and Engineering, Vol. 55, pp. 301-320.

Taylor, L. M., and D. P. Flanagan, 1987, "PRONTO 2D - A Two-Dimensional Transient Solid Dynamics Program," Sandia National Laboratories Report SAND86-0594, Albuquerque, New Mexico.

Thorne, B. J., 1990, "A Damage Model for Rock Fragmentation and Comparison of Calculations with Blasting Experiments in Granite," Sandia National Laboratories Report SAND90-1389, Albuquerque, New Mexico.

Thorne, B. J., 1991, "Application of a Damage Model for Rock Fragmentation to the Straight Creek Mine Blasting Experiments," Sandia National Laboratories Report SAND91-0867, Albuquerque, New Mexico.

DISCLAIMER